Homogeneous and heterogeneous nucleation of Lennard-Jones liquids

Hui Wang and Harvey Gould
Department of Physics, Clark University, Worcester, Massachusetts 01610, USA

W. Klein
Department of Physics, Boston University, Boston, Massachusetts 02215, USA

(Received 30 May 2007; published 25 September 2007)

The homogeneous and heterogeneous nucleation of a Lennard-Jones liquid is investigated using the umbrella sampling method. The free energy cost of forming a nucleating droplet is determined as a function of the quench depth, and the saddle point nature of the droplets is verified using an intervention technique. The structure and symmetry of the nucleating droplets are found for a range of temperatures. We find that for deep quenches the nucleating droplets become more anisotropic and diffuse with no well-defined core or surface. The environment of the nucleating droplets forms randomly stacked hexagonal planes. This behavior is consistent with a spinodal nucleation interpretation. We also find that the free energy barrier for heterogeneous nucleation is a minimum when the lattice spacing of the impurity equals the lattice spacing of the equilibrium crystalline phase. If the lattice spacing of the impurity is different, the crystal grows into the bulk instead of wetting the impurity.

DOI: 10.1103/PhysRevE.76.031604 PACS number(s): 64.60.Qb, 82.60.Nh

I. INTRODUCTION

Although crystallization from a supercooled liquid has been the subject of extensive simulations [1–6], theory [7–11], and experiments [12,13], the nature of the nucleating droplet in supercooled liquids is not well understood, especially for deep quenches. For shallow quenches (near coexistence), classical nucleation theory applies. For deeper quenches, nucleation is affected by the proximity to the liquid-solid spinodal for systems with long-range interactions [10]. The spinodal represents the limit of stability of the metastable liquid and is well defined only in the limit of an infinite interaction range. However, spinodal-like effects have been found for deep quenches in systems with intermediate and short-range interactions [1,14,15]. Spinodal nucleation theory predicts that the decrease of the surface tension of the droplets as the spinodal is approached makes the nucleating droplets diffuse and fractal-like. Moreover, the symmetry of the nucleating droplets is not necessarily the same as the symmetry of the stable phase, and the symmetry of the nucleating droplets in three dimensions is either body-centered cubic (bcc) or randomly stacked hexagonal planes. Trudu *et al.* [15] studied nucleation of a Lennard-Jones liquid using transitional path sampling and found a crossover from classical to spinodal-like behavior for deeper quenches. In particular, they observed that the nucleating droplets become less compact and spherical, but did not analyze the structure and symmetry of the nucleating droplets.

The study of heterogeneous nucleation—that is, nucleation that occurs on impurities—is of much practical importance because most nucleation events that occur in nature are heterogeneous. Examples include nucleation on a container wall [16] and nucleation of proteins in porous media [17]. Many experiments [18,19] and simulations [20–22,11] have been done to study heterogeneous nucleation. Existing theories of heterogeneous nucleation are mostly phenomenological and natural extensions of classical nucleation theory [23–25]. It is known that the presence of impurities can lower the free energy barrier of nucleation by as much as several orders of magnitude [20]. The effectiveness of an impurity to decrease the nucleation barrier is determined by properties such as the shape of the impurity and the surface tension between the substrate and the metastable liquid. Page and Sear [21] studied heterogeneous nucleation in porous media using the Ising model and found that a pore which is approximately the size of the critical nucleus is most effective for decreasing the nucleation barrier. Heterogeneous nucleation on a structureless solid surface has also been simulated [16]. However, the effects of the microscopic properties of the impurities on nucleation have not been well characterized.

In this paper, we will study homogeneous and heterogeneous nucleation in supercooled Lennard-Jones liquids using the umbrella sampling method. For homogeneous nucleation, we find spinodal effects for deep quenches by analyzing the structure of the nucleating droplets. In particular, the nucleating droplets are found to become more anisotropic and diffuse with no well-defined core or surface. The droplets and their immediate environment form randomly stacked hexagonal planes, which is consistent with the spinodal nucleation picture.

To study heterogeneous nucleation a fixed impurity consisting of particles that form a hexagonal plane is added to the system. We find that the impurity whose lattice spacing is equal to the lattice spacing of the equilibrium crystalline phase is most effective in lowering the free energy barrier of nucleation. We also find that when the lattice spacing of the impurity is different than the optimal spacing, the crystal prefers to nucleate on the newly formed crystal (grow into the bulk) instead of wetting the impurity.

This paper is organized as follows. Section II describes the simulation details and the intervention technique which we use to test the saddle point nature of the nucleating droplets. Section III presents the simulation results of homogeneous nucleation, and Sec. IV discusses our results on heterogeneous nucleation.

II. SIMULATION DETAILS

The three-dimensional system of interest consists of $N=4000$ particles with density $\rho=0.95$ interacting via the Lennard-Jones potential. Periodic boundary conditions are used. We adopt dimensionless units so that lengths and energies are given in terms of the Lennard-Jones parameters σ and ϵ. We first prepared a liquid at $T=1.20$, which is above the coexistence temperature ($T_m \approx 1.15$ [26]), by melting a perfect face-centered cubic (fcc) crystal; this simulation is done using the Metropolis algorithm at constant volume. The system is equilibrated for 50 000 Monte Carlo steps per particle (MCS) in the liquid phase before the quench. The system is then quenched by rescaling the temperature by a factor of 0.999 every 20 MCS per particle.

Because the probability of nucleation is very small, we used the umbrella sampling method [27–31]. We denote ϕ as the order parameter, which we choose to be the number of particles in the largest (solidlike) cluster. (The definition of the solidlike clusters is discussed in Sec. II A.) The free energy $G(\phi)$ is calculated from the relation

$$G(\phi) = -k_B T \ln P(\phi), \tag{1}$$

where $P(\phi)$ is the probability density of ϕ.

In the umbrella sampling method, the system is sampled according to the total potential energy $\tilde{V}=V+V_b(\phi)$, where V is the original potential energy of the system and $V_b(\phi)$ is the bias potential. The probability distribution $\tilde{P}(\phi)$ is sampled according to the total density operator $\tilde{\rho}=e^{-\beta V}e^{-\beta V_b(\phi)}=\rho_0 e^{-\beta V_b(\phi)}$, which is the product of the original density operator ρ_0 and the weight function due to the bias $e^{-\beta V_b(\phi)}$. The original distribution $P(\phi)$ can be determined by

$$P(\phi) = \tilde{P}(\phi) e^{\beta V_b(\phi)}. \tag{2}$$

The free energy $G(\phi)$ in Eq. (1) can be calculated by

$$G(\phi) = -k_B T \ln \tilde{P}(\phi) - V_b(\phi). \tag{3}$$

As in Ref. [27], the potential bias has the form

$$V_b(\phi) = \frac{1}{2} k (\phi - \phi_0)^2. \tag{4}$$

The constant $k=0.05$ determines the width of the sampling window and yields $\Delta\phi \approx 15$. We consider a sequence of values of ϕ_0 starting from size 0 and increasing by ten particles—that is, $\phi_0 = 0, 10, 20, \ldots$. Because the width of the window $\Delta\phi \approx 15$, the choice of ten particles means that the sampling windows overlap. Before collecting data for the probability $\tilde{P}(\phi)$ for each value of ϕ_0, the system is equilibrated for 10 000 MCS. The values of ϕ are then sampled for 100 000 MCS. To save equilibration time a configuration for the current value of ϕ_0 is used as the initial condition for the next value of ϕ_0. Because determining the size of the largest cluster is computationally expensive, we make trial moves for 5 MCS using only the Lennard-Jones potential without the bias potential and then accept or reject these trial moves using only the bias potential in Eq. (4).

A. Cluster analysis

Unlike the Ising and Potts models [32] there is no rigorous definition of clusters in a continuous particle system. Instead we are forced to rely on our intuition to identify the solidlike particles. We use the local bond-order analysis introduced by Steinhardt *et al.* [33] and developed by Frenkel and co-workers [31]. We define the $(2l+1)$-component complex vector $\bar{q}_{lm}(i)$ for particle i:

$$\bar{q}_{lm}(i) = \frac{1}{n_i} \sum_{j=1}^{n_i} Y_{lm}(\hat{r}_{ij}), \tag{5}$$

where the sum is over the n_i nearest neighbors of particle i and $Y_{lm}(\hat{r}_{ij})$ is the spherical harmonic as a function of the unit direction vector $\hat{r}_{ij}$ between particle i and its n_i nearest neighbors. The nearest neighbors of a given particle are defined to be within the distance 1.4, which corresponds to the position of the first minimum of the radial distribution function of the crystalline phase at the same density and temperature.

It has been shown that $l=6$ is a good choice for characterizing the structures of crystals [28]. The rotational invariants $w_4(i)$, $w_6(i)$, $q_4(i)$, and $q_6(i)$ are defined as

$$q_l(i) = \left(\frac{4\pi}{2l+1} \right) \left(\sum_{m=-l}^{l} |\bar{q}_{lm}(i)|^2 \right)^{1/2} \tag{6}$$

and

$$w_l(i) = \frac{\bar{w}_l(i)}{\left[\sum_{m=-l}^{l} |\bar{q}_{lm}(i)|^2 \right]^{3/2}}, \tag{7}$$

with

$$\bar{w}_l(i) = \sum_{m_1+m_2+m_3=0} \begin{pmatrix} l & l & l \\ m_1 & m_2 & m_3 \end{pmatrix} \bar{q}_{lm_1}(i) \bar{q}_{lm_2}(i) \bar{q}_{lm_3}(i). \tag{8}$$

The quantity in brackets in Eq. (8) is Wigner's $3j$ symbol.

To define a solidlike particle, we first introduce the normalized quantity $\tilde{q}_{lm}(i)$ as

$$\tilde{q}_{lm}(i) = \frac{\bar{q}_{lm}(i)}{\left[\sum_{m=-l}^{l} |\bar{q}_{lm}(i)|^2 \right]^{1/2}}, \tag{9}$$

and form the dot product

$$c_{ij} = \sum_{m=-6}^{6} \tilde{q}_{6m}(i) \tilde{q}_{6m}(j)^*, \tag{10}$$

where an asterisk (*) indicates the complex conjugate. The dot product $c_{ii}=1$ by construction. Particles i and j are said to be *coherent* if the real part of the dot product c_{ij} is greater than 0.5. A particle is considered to be solidlike if its number of coherent neighbors is greater than or equal to n_b. We will chose $n_b=11$ for reasons that we will discuss in Sec. II B. After finding all the solidlike particles, we construct the clus-

ters using the criterion that any two solidlike particles that are nearest neighbors [see their definition after Eq. (5)] belong to the same cluster.

As discussed in Ref. [31], the distribution of the invariants $q_4(i)$, $w_6(i)$, and $q_6(i)$ can be used to characterize the symmetry of a group of particles—for example, a cluster. For a given group of particles we first determine the histogram of each invariant. The three histograms are then rescaled so that they do not overlap and are combined to form the histogram H. The histogram H corresponding to a group of particles is decomposed in terms of the histograms of the invariants corresponding to the symmetries of interest—namely, fcc, bcc, and hcp (hexagonal close-packed):

$$H = f_{\mathrm{fcc}} H_{\mathrm{fcc}} + f_{\mathrm{bcc}} H_{\mathrm{bcc}} + f_{\mathrm{hcp}} H_{\mathrm{hcp}}. \tag{11}$$

For example, H_{fcc} is determined for a system with fcc symmetry in which a certain amount of randomness has been introduced [34]. The coefficients corresponding to each symmetry, f_{fcc}, f_{bcc}, and f_{hcp}, are found by minimizing the quantity

$$(H - f_{\mathrm{fcc}} H_{\mathrm{fcc}} - f_{\mathrm{bcc}} H_{\mathrm{bcc}} - f_{\mathrm{hcp}} H_{\mathrm{hcp}})^2, \tag{12}$$

with the constraints that $f_{\mathrm{fcc}}, f_{\mathrm{bcc}}, f_{\mathrm{hcp}} > 0$ and $f_{\mathrm{fcc}} + f_{\mathrm{bcc}} + f_{\mathrm{hcp}} = 1$. The coefficients f_{fcc}, f_{bcc}, and f_{hcp} are indications of the composition of each symmetry associated with the group particles.

B. Intervention method

Because the cluster analysis involves parameters such as the minimum number of coherent neighbors, the computed size of the clusters depends somewhat on the values chosen for the parameters. To determine if our choices are consistent, we use the fact that the nucleating droplets correspond to the maximum of the free energy barrier and should be saddle point objects; that is, the nucleating droplets should grow or shrink with approximately 50% probability under a small perturbation. In practice, the cluster analysis parameters are first chosen and the umbrella sampling procedure is performed. Then the intervention method is used to test if intervention causes the clusters corresponding to the maximum of the free energy to grow or shrink with ≈50% probability. If these clusters do not, the parameters in the cluster analysis are modified until approximately 50% growth probability is achieved for the modified clusters at the new free energy maximum.

The intervention method we adopt is similar to what has been used to study nucleation in the Ising model [35,36]. To test if a cluster is a nucleating droplet, we run the simulation at the free energy maximum (see Sec. III) and then stop the simulation and make many copies of a typical configuration. Each copy is restarted with a different random number seed without the potential bias. We then determine if the largest cluster in each copy grows at approximately the same place at approximately the same time as the original. After the time t_{obs}, both the size and location of the cluster are examined. If the size of the cluster is larger than its original size and the center of mass is within a distance r^* from the cluster in the original configuration, the cluster is said to grow. The role of r^* is to ensure that the cluster is the same as the one in the original configuration. We choose $t_{\mathrm{obs}} = 10\,000$ MCS. The distance r^* should correspond to the size of the cluster; typically 50% of the linear spatial extent of the cluster is sufficient to decide whether the cluster kept its identity during t_{obs}. Because intervention is very time consuming, we made 20 copies of each configuration. By determining the frequency of the successful trials we can estimate the probability of growth of a cluster. The fraction of trials (out of 20 trials) for which the cluster grows is listed in Table I for different temperatures. We found that setting $n_{\mathrm{b}} = 11$ gives consistent results.

TABLE I. Fraction of the copies of the nucleating droplets that grow after intervention (out of 20). These results indicate that the clusters that are generated at the maximum of the free energy correspond to nucleating droplets.

T	Fraction	T	Fraction
0.75	0.65	0.60	0.40
0.70	0.60	0.55	0.45
0.65	0.35	0.53	0.55

III. HOMOGENEOUS NUCLEATION

We determined $G(\phi)$ at several temperatures between $T = 0.75$ and $T = 0.53$. As expected, $G(\phi)$ exhibits a minimum and a maximum [see Fig. 1(a)]. The minimum of G corresponds to the metastable supercooled liquid in which solid-

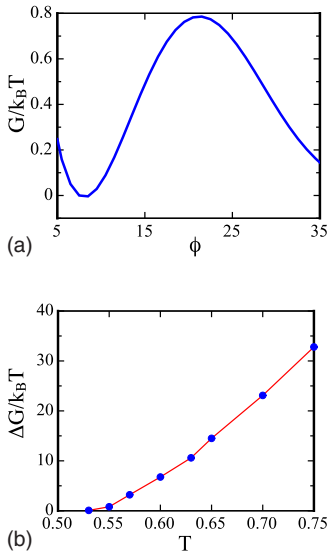

FIG. 1. (Color online) (a) The Gibbs free energy as a function of the order parameter ϕ, the size of the largest cluster in the system, at $T = 0.55$. The minimum of G corresponds to the metastable supercooled liquid phase, and the maximum corresponds to the nucleating droplet. The free energy minimum is at $\phi \approx 7$, showing that there are some solidlike particles in the supercooled liquid state. (b) The nucleation barrier as a function of the temperature. The barrier apparently vanishes at $T \approx 0.53$.

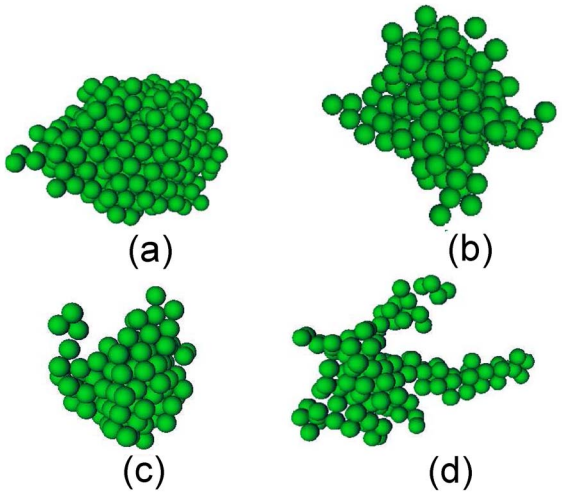

FIG. 2. (Color online) Snapshots of the nucleating droplet at temperatures (a) $T=0.75$, (b) $T=0.65$, (c) $T=0.60$, and (d) $T=0.55$.

like particles are present due to thermal fluctuations. The maximum occurs at the size of the nucleating droplet (recall that we have chosen the order parameter to be the size of the largest cluster). The free energy difference of the maximum and minimum can be interpreted as the free energy barrier ΔG for nucleation [27]. We find that the nucleation barrier decreases with temperature [see Fig. 1(b)] and vanishes at $T \approx 0.53$. This vanishing of the free energy barrier raises questions as to whether or not it corresponds to a spinodal.

The spinodal is usually defined as the sharp boundary between the metastable and unstable states [37,38]. In particular, the spinodal is a thermodynamic transition that acts as a line of critical points. (In Ising models the spinodal corresponds to a divergent isothermal susceptibility [39,40].) We will refer to this interpretation as the classical spinodal [41,42]. The spinodal as defined in this way is present only in mean-field systems such as those with infinite range interactions. Systems with long but finite-range interactions can exhibit pseudospinodal effects similar to those seen at the spinodal [37–40,43–45].

To test if $T=0.53$ corresponds to the classical spinodal we also simulated the system at this temperature by a standard Metropolis algorithm. By tracking the size of the largest cluster we found that the lifetime of the metastable state is in the range $[1\times10^5, 6\times10^5]$ MCS, which implies that the free energy barrier to nucleation has not vanished at $T=0.53$. Hence the vanishing of the free energy barrier found by umbrella sampling does not necessarily correspond to a classical spinodal. Moreover, we found (see Table I) that the droplets found by umbrella sampling appear to be saddle point objects as determined by the intervention method (without the bias potential). A possible explanation is that the interpretation of the umbrella sampling results for $P(\phi)$ assumes that clusters whose size are comparable to the nucleating droplet are rare [27]. This assumption is not applicable for $T \approx 0.53$ because there is typically more than one large cluster of comparable size in the system. We will investigate this assumption and other possible explanations in future work.

Figure 2 shows snapshots of the nucleating droplet at different temperatures. Note that the droplets are compact for moderate supercooling and become more diffuse for deeper quenches. This qualitative observation is consistent with Ref. [15]. We will analyze the structure of the nuclei in the following.

A. Structure of the nucleating droplets

To measure the compactness of a nucleating droplet, we determine its density profile $\rho(r)$, which is defined in terms of the mean number of particles, $N(r)$, in the spherical shell between r and $r+dr$:

$$N(r) = \rho(r) 4\pi r^2 dr. \tag{13}$$

Here r is measured from the center of mass of a nucleating droplet.

Figure 3 shows $\rho(r)$ averaged over 1000 nucleating droplets at the value of ϕ_0 corresponding to the maximum of $G(\phi)$. For $T=0.75$, $\rho(r)$ has a plateau for small r, meaning that the droplet has a well-defined core. The decrease of $\rho(r)$ for larger r indicates that there is an interface between the core and liquid environment. At $T=0.55$, the plateau disappears and the density slowly decreases from the core to the surface, indicating that the nucleating droplet is diffuse.

To quantify the anisotropy of the nucleating droplets, we calculate the moment of inertia tensor associated with each droplet,

$$I_{\alpha\beta} = \sum_{i=1}^{n} (r_i^2 \delta_{\alpha\beta} - r_{i,\alpha} r_{i,\beta}), \tag{14}$$

where $r_i^2 = \Sigma_\alpha r_{i,\alpha} r_{i,\alpha}$, i labels the particles and α and β label the components of $\vec{r}$. The square root of the eigenvalues of $I_{\alpha\beta}$ defines the principal radii of the ellipsoid characterizing the droplet. The orientation of each individual nucleating droplet is found to be random; that is, the long axis of the

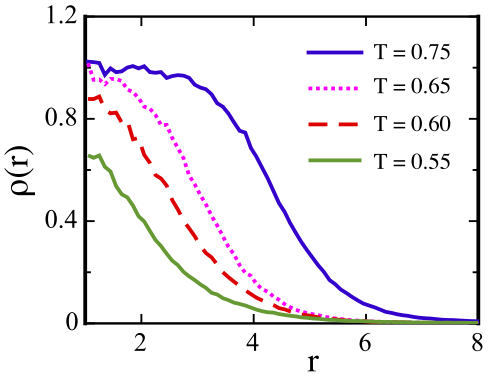

FIG. 3. (Color online) The density profile $\rho(r)$ of the nucleating droplets for various temperatures. At $T=0.75$, the nucleating droplet has a well-defined core corresponding to the plateau of $\rho(r)$. Note that the density at the core is slightly higher than 0.95, the mean density. The decrease of $\rho(r)$ for larger r implies that there is a well-defined interface between the core and the liquid environment. At lower temperatures, the plateau disappears and the density gradually decreases as r increases, suggesting that the nucleating droplet are more diffuse.

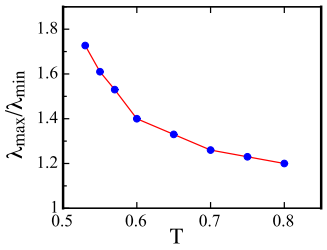

FIG. 4. (Color online) The ratio of the maximum and minimum of the eigenvalues of the moment of inertia tensor of the nucleating droplets. The increase of the ratio at low temperatures indicates that the nucleating droplets become more anisotropic.

computed ellipsoid points in random directions independent of the orientations of the simulation cell. We can characterize each droplet's anisotropy by calculating the ratio of the maximum and minimum principal radii (denoted by λ_{max} and λ_{min}, respectively). This ratio is 1 for a perfectly spherical droplet and is greater than 1 if the droplet is anisotropic. Figure 4 shows the ratio (averaged over 1000 nucleating droplets at each temperature) as a function of the temperature. The ratio is close to one for shallow quenches, meaning that the nucleating droplets are close to spherical. The increase of the ratio at lower temperatures indicates that the nucleating droplets become more anisotropic. The anisotropic character of the nucleating droplets is important in the calculation of the nucleation barrier even in classical nucleation theory [15].

Figure 5 shows that the number of particles, n_c, in the nucleating droplet and the radius of gyration, R_g, decrease as the temperature is decreased. Both quantities are predicted to first decrease as the temperature is lowered from coexistence and then begin to increase as the spinodal is approached [46]. In particular, if the spinodal interpretation is applicable, simple scaling arguments [47] suggest that n_c (in three dimensions) and R_g (in all dimensions) should increase as the spinodal is approached if the system is sufficiently close to the spinodal so that the core of the nucleating droplet has disappeared. The fact that n_c and R_g do not increase rapidly at lower temperatures in our simulations might be due to the nonexistence of spinodal effects and/or the underestimate of n_c and R_g near the spinodal due to our *ad hoc* definition of solidlike particles. A more likely explanation is that because the nucleating droplets near the spinodal are anisotropic and effectively two dimensional, simple scaling arguments do not apply. In Fig. 5(b) we plot the semimajor axis λ_{max} of the nucleating droplets. Note that λ_{max} does show the expected increase. In addition, the scaling arguments [47] in two dimensions suggest that n_c is either a constant or is logarithmically divergent as the spinodal is approached. More work is needed to understand the temperature dependence of n_c, R_g, and λ_{max} in the intermediate region where neither the classical nor spinodal picture is applicable.

B. Symmetry of the nucleating droplets

The symmetry of the nucleating droplets is analyzed using the method discussed in Sec. II A. At each temperature, we

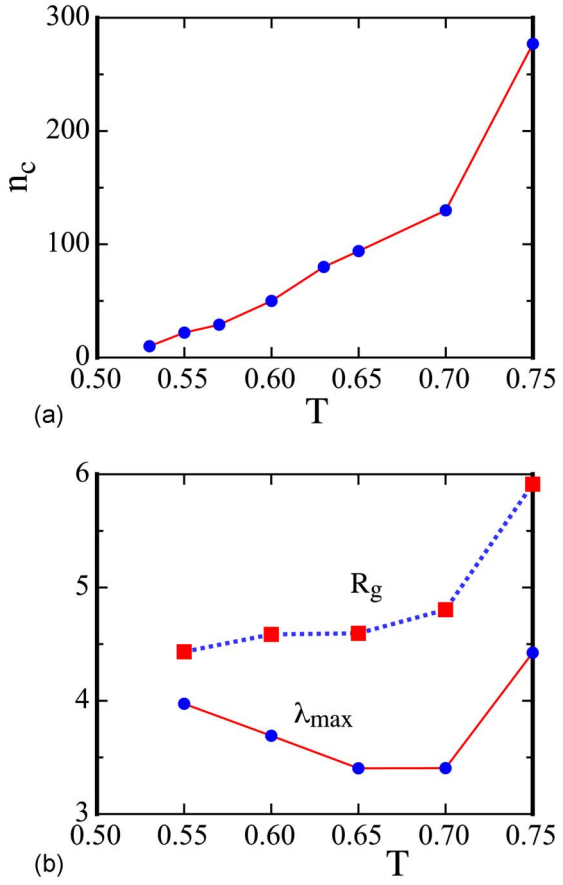

FIG. 5. (Color online) (a) The mean number of particles in the nucleating droplets as a function of T. (b) The radius of gyration, R_g, and mean semimajor axis λ_{max} of the nucleating droplets. The data are averaged over 1000 independent configurations. Note that the λ_{max} increases as T is decreased below $T \approx 0.65$.

obtain the parameters f_{fcc}, f_{bcc}, and f_{hcp} for the nucleating droplets averaged over 1000 independent configurations. The fitting parameters are listed in Table II and are plotted in Fig. 6. As the temperature is decreased, the fcc component decreases and the bcc and hcp components increase. The mixture of fcc and hcp components signifies the occurrence of the rhcp (random hybrid close-packed) structure [13] and is consistent with the picture of stacked hexagonal planes [10].

We also calculated the symmetry of the particles in a spherical shell between r and $r+\Delta r$, where r is measured from the center of mass of the cluster and Δr is the thickness

TABLE II. Values of the coefficients corresponding to the symmetry of the nucleating droplets for different temperatures.

T	f_{fcc}	f_{hcp}	f_{bcc}
0.75	0.62	0.38	0.00
0.70	0.50	0.48	0.02
0.65	0.46	0.52	0.02
0.60	0.28	0.66	0.06
0.55	0.26	0.68	0.06

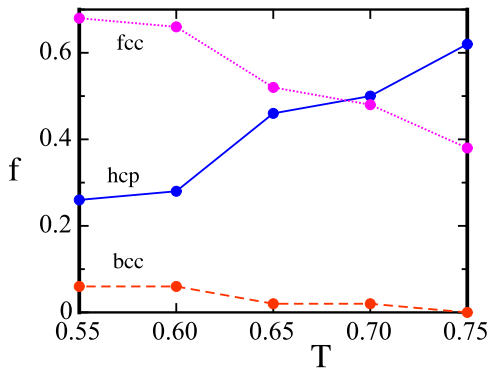

FIG. 6. (Color online) The coefficient f of each symmetry of the nucleating droplet as a function of temperature. The results are averaged over 1000 independent configurations. As the temperature is decreased, the hcp and bcc components increase and the fcc component decreases.

of the shell ($\Delta r=0.2$). Figure 7 shows the component of each structure as a function of r for various temperatures. At $T=0.75$, the core of the nucleating droplet is mostly fcc. Away from the center, the fcc component decreases and the bcc and liquid component increases. At the surface, the bcc component levels off to $f_{\mathrm{bcc}} \approx 0.1$. The fact that the nucleating droplet is composed of an fcc core and a bcc halo agrees with previous results [31]. At $T=0.55$ the nucleating droplet is mainly a mixture of fcc and hcp components, with a slight increase of the bcc component. The increase of bcc symmetry and decreased distinction between the bulk and the surface for deep quenches are in agreement with the spinodal nucleation picture [10].

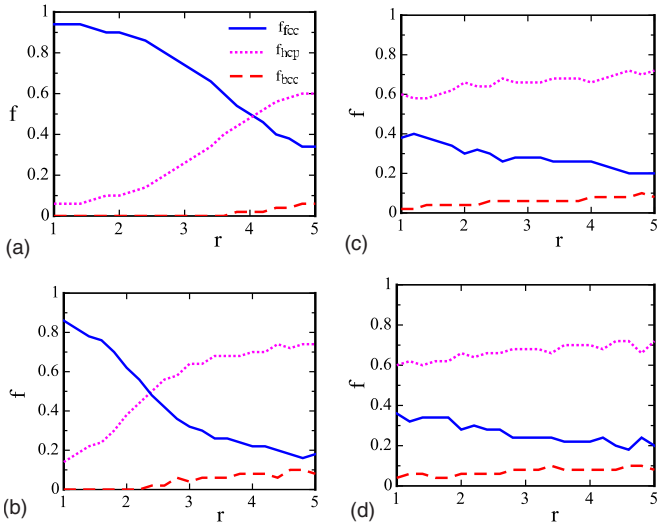

FIG. 7. (Color online) The component of each symmetry as a function of the distance r from the center of mass of the nucleating droplets at temperatures (a) $T=0.75$, (b) $T=0.65$, (c) $T=0.60$, and (d) $T=0.55$. The results are averaged over 1000 configurations. At $T=0.75$ the core of the nucleus is predominately fcc and the surface shows some bcc and liquid symmetry. At $T=0.55$ the fcc symmetry is less dominant for small r and the bcc component for small r is close to its value for larger r.

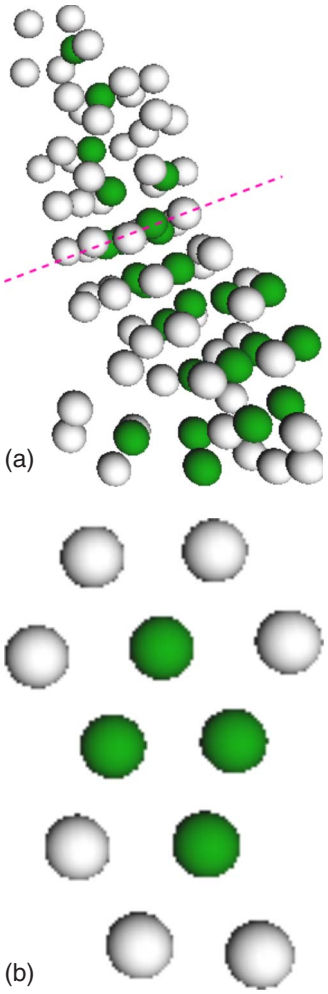

FIG. 8. (Color online) (a) Snapshot of a nucleating droplet (dark particles) and particles in the local environment (light particles) at $T=0.55$. (b) The layer of particles corresponding to the plane indicated by the dashed line in (a) forms a hexagonal structure.

We also examined the structure of the particles in the nucleating droplet and its local environment, which consists of particles that are nearest neighbors of any particle in the droplet. Although the particles in the nucleating droplets by themselves do not seem to form a visually identifiable struc-

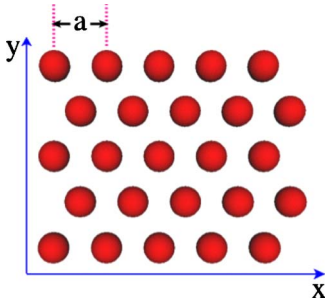

FIG. 9. (Color online) Sketch of the impurity used to study heterogeneous nucleation. The area of the impurity is $A=\frac{\sqrt{3}}{2}mna^2$, where m and n are the number of particles in the x and y directions, respectively.

TABLE III. Values of m and n used to study the effect of changing the lattice spacing. The area of the impurity is fixed.

$m \times n$	Lattice spacing a	$\Delta G/k_B T$
6×6	0.908	37
5×6	0.995	22
5×5	1.090	3.3
4×5	1.218	20
4×4	1.360	30

ture, the nucleating droplets and the surrounding particles in the liquid phase together form hexagonally stacked planes (see Fig. 8).

IV. HETEROGENEOUS NUCLEATION

To study heterogeneous nucleation, an impurity of $m \times n$ Lennard-Jones particles in a hexagonal plane is placed into the system, where m and n are the number of particles in the x and y directions (see Fig. 9). The z direction is perpendicular to the plane of the impurity. The positions of the particles in the impurity are fixed during the simulation. The impurity is characterized by its lattice spacing a and total area $A = \frac{\sqrt{3}}{2} mna^2$. The efficiency of the impurity is measured by the height of the nucleation barrier ΔG, which we compute as before using the umbrella sampling method.

If the system is crystallized homogeneously after a quench to $T < T_m$, the position of the first peak of the radial distribution function $g(r)$ is ≈ 1.09. We take the value $a_s = 1.09$ as the lattice spacing of the solid phase. The temperature is quenched to $T=0.75$, which corresponds to the region where classical nucleation applies in the absence of an impurity (see Sec. III). At $T=0.75$ the free energy barrier of homogeneous nucleation is $\Delta G/k_B T \approx 40$ in the absence of an impurity with $n_c \approx 300$. In all of our simulations of heterogeneous nucleation, nucleation always occurs on the impurity if it is present.

We studied the dependence of the nucleation barrier on the lattice spacing for fixed area A, which is chosen to be $A = \frac{\sqrt{3}}{2}(5 \times 1.09)^2$, the area of a 5×5 impurity with lattice spacing $a_s = 1.09$. The impurities have different values of m and n so that their lattice spacings are less than and greater than a_s (see Table III). The free energy barrier is lowest at

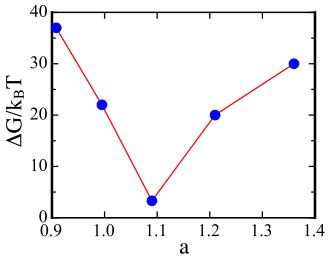

FIG. 10. (Color online) The free energy barrier as a function of the lattice spacing a for fixed area $A = \frac{\sqrt{3}}{2}(5 \times 1.09)^2$. The nucleation barrier is a minimum at $a = a_s$.

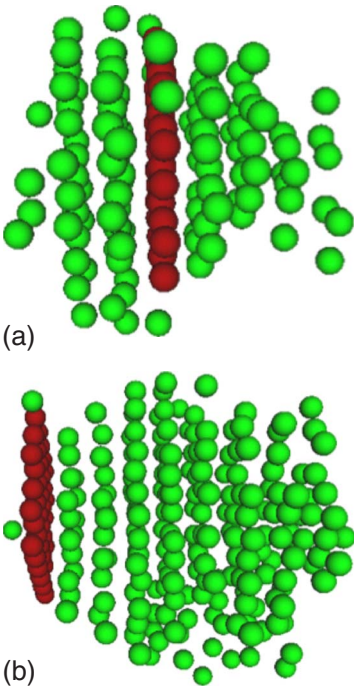

FIG. 11. (Color online) Snapshots of nucleating droplets in the presence of an impurity with (a) $a=1.09$ and (b) $a=0.908$. The dark particles are the impurity; the size of the nucleating droplets is 146 and 250 particles, respectively. For $a=1.09$ the nucleating droplet grows on both sides of the impurity. Once the impurity initiates nucleation for $a=0.908$, it is preferential to add particles on the newly formed droplet than wetting the other side of the impurity.

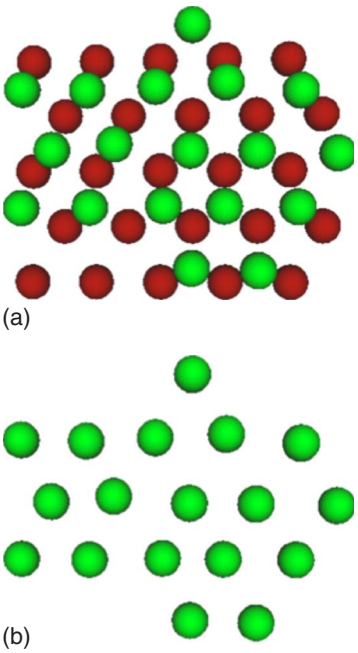

FIG. 12. (Color online) Snapshots of the first layer of the nucleating droplet in the presence of a 5×5 impurity at $a = a_s$. The layer of the nuclei lies on top of the impurity (dark particles). Within the layer the solidlike particles form a hexagonal structure. (b) Same snapshot as (a) with particles in the impurity not shown.

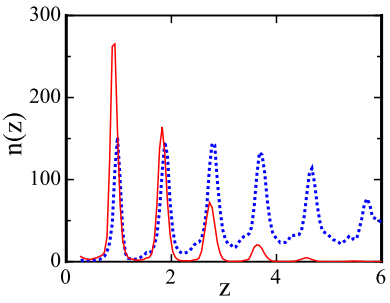

FIG. 13. (Color online) Number of particles in the nucleating droplets as a function of z. The solid line is for a 5×5 impurity with $a=1.09$, and the dotted line is for a 6×6 impurity with $a=0.908$.

$a\approx a_s$ (see Fig. 10); that is, an impurity is most efficient in lowering the nucleation barrier if its lattice spacing is the same as that of the crystalline phase.

By investigating snapshots of the nucleating droplets we found that in general the nucleating droplet forms on both sides of the impurity for $a\approx a_s$ [see Fig. 11(a)]. For $a\neq a_s$, once the impurity initiates nucleation, it becomes preferential to add particles on the newly formed droplet than on the impurity, making the droplet grow into the bulk instead of wetting the other side of the impurity. In both cases the nucleating droplets grow on the impurity by forming layered planes, with each layer being parallel to the plane of the impurity. Inside each layer the solidlike particles form a hexagonal structure (Fig. 12). The lattice spacing of the nucleating droplets is approximately a_s, irrespective of the lattice spacing of the impurity. That is, once a nucleus is formed, its lattice spacing becomes very close to the optimal spacing a_s and the droplets form on the newly formed layer rather than on the impurity.

A simple way to characterize how the nucleating droplet wets the impurity is to measure its profile. In Fig. 13 we show the number of particles in the nucleating droplet, $n(z)$, as a function of z, where z is the distance of a particle from the plane of the impurity. The sharp peaks of $n(z)$ indicate that the nuclei form a layered structure. For $a=1.09$ $n(z)$ gradually drops to zero as z increases. In contrast, $n(z)$ is almost flat for $a=0.908$. The protrusion of the nuclei into the bulk for $a=0.908$ is consistent with the fact that the nucleating droplet wets the impurity at $a=a_s$ and grows into the bulk when $a\neq a_s$.

Contour plots of the profile were obtained by projecting the density of the nuclei onto the x-z plane. Figure 14 shows contour plots for impurities with $a=1.09$ and $a=0.908$, respectively. The smaller contact angle for the impurity with $a=1.09$ is consistent with the fact that it is preferential to nucleate on the impurity when its lattice spacing is optimal.

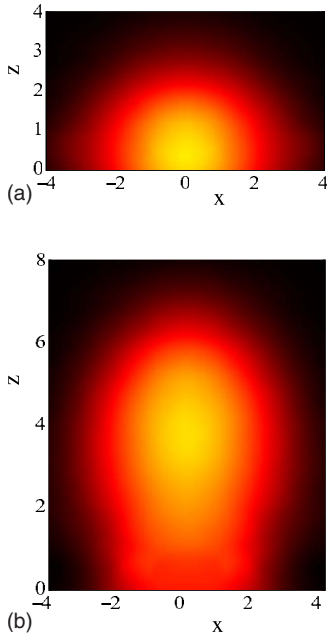

FIG. 14. (Color online) Contour plots of the nucleating droplets in the presence of an impurity. The impurity is at $z=-1$ and the density of the nuclei is projected onto the x-z plane. The plots are obtained by averaging over 200 independent configurations of the nucleating droplets. (a) The lattice spacing of the impurity is $a=1.09$, with $n_c=150$. (b) The lattice spacing is $a=0.908$ with $n_c=300$. The smaller contact angle of the impurity with $a=1.09$ is consistent with the fact that it is preferential to nucleate on the impurity when its lattice spacing is optimal.

V. CONCLUSIONS

We studied the homogeneous and heterogeneous nucleation of Lennard-Jones liquids using the umbrella sampling method. By analyzing the symmetries of the nucleating droplets, we found that for deep quenches the nucleating droplets are more diffuse and anisotropic with no well-defined core or surface; the nucleating droplets and the corresponding liquid environment form randomly stacked hexagonal planes. These results are consistent with the spinodal nucleation picture. For heterogeneous nucleation, we found that the droplets grow on an impurity of hexagonal plane by layers and the solidlike particles in each layer form a hexagonal structure. For a fixed area of the impurity, the free energy barrier of nucleation is a minimum when the lattice spacing of the impurity is equal to a_s, the lattice spacing of the equilibrium crystalline phase. The lattice spacing of the nuclei is equal to a_s even when the lattice spacing of the impurity is different than a_s, and it is favorable for the nucleating droplets to grow into the bulk instead of wetting the impurity.

[1] Ju-xing Yang, H. Gould, and W. Klein, Phys. Rev. Lett. **60**, 2665 (1988).
[2] W. C. Swope and H. C. Andersen, Phys. Rev. B **41**, 7042 (1990).
[3] M. Matsumoto, S. Saito, and I. Ohmine, Nature (London) **416**, 409 (2002).
[4] J. Delhommelle, J.-M. Leyssale, and C. Millotc, J. Chem. Phys. **122**, 104510 (2005).
[5] J. Yang, H. Gould, W. Klein, and R. Mountain, J. Chem. Phys. **93**, 711 (1990).
[6] F. J. Cherne, M. I. Baskes, R. B. Schwarz, S. G. Srinivasan, and W. Klein, Modell. Simul. Mater. Sci. Eng. **12**, 1063 (2004).
[7] Y. C. Shen and D. W. Oxtoby, J. Chem. Phys. **105**, 6517 (1996).
[8] S. Alexander and J. McTague, Phys. Rev. Lett. **41**, 702 (1978).
[9] W. Klein, Phys. Rev. E **64**, 056110 (2001).
[10] W. Klein and F. Leyvraz, Phys. Rev. Lett. **57**, 2845 (1986).
[11] Mario Castro, Phys. Rev. B **67**, 035412 (2003).
[12] E. Thune, Th. Cabioch, M. Jaouen, and F. Bodart, Phys. Rev. B **68**, 115434 (2003).
[13] A. Schofield, P. N. Pusey, D. A. Weitz, U. Gasser, and E. R. Weeks, Science **292**, 258 (2001).
[14] D. W. Heermann and W. Klein, Phys. Rev. Lett. **50**, 1062 (1983).
[15] F. Trudu, D. Donadio, and M. Parrinello, Phys. Rev. Lett. **97**, 105701 (2006).
[16] S. Toxvaerd, J. Chem. Phys. **117**, 10303 (2002).
[17] E. Saridakis, N. E. Chayen, and R. P. Sear, Proc. Natl. Acad. Sci. U.S.A. **103**, 597 (2006).
[18] Yadong Yin and Younan Xia, Adv. Mater. (Weinheim, Ger.) **13**, 267 (2000).
[19] P. W. Wilson, A. F. Heneghan, and A. D. J. Haymet, Proc. Natl. Acad. Sci. U.S.A. **99**, 9631 (2002).
[20] S. Auer and D. Frenkel, Phys. Rev. Lett. **91**, 015703 (2003).
[21] A. J. Page and R. P. Sear, Phys. Rev. Lett. **97**, 065701 (2006).
[22] L. Gránásy, T. Pusztai, D. Saylor, and J. A. Warren, Phys. Rev. Lett. **98**, 035703 (2007).
[23] Zhen-Gang Wang, Jiafang Wang, and Yuliang Yang, J. Chem. Phys. **121**, 1105 (2004).
[24] H. Vehkamäki, A. Lauri, E. Zapadinsky, and M. Kulmala, J. Chem. Phys. **125**, 164712 (2006).
[25] Y. Djikaev and E. Ruckenstein, J. Chem. Phys. **125**, 244707 (2006).
[26] J.-P. Hansen and L. Verlet, Phys. Rev. **184**, 151 (1969).
[27] S. Auer and D. Frenkel, J. Chem. Phys. **120**, 3015 (2004).
[28] J. S. van Duijneveldt and D. Frenkel, J. Chem. Phys. **96**, 4655 (1992).
[29] G. Torrie and J. Valleau, Chem. Phys. Lett. **28**, 578 (1974).
[30] G. Torrie and J. Valleau, J. Comput. Phys. **23**, 187 (1977).
[31] D. Frenkel, P. R. ten Wolde, and M. J. Ruiz-Montero, J. Chem. Phys. **104**, 9932 (1996).
[32] A. Coniglio and W. Klein, J. Phys. A **13**, 2775 (1980).
[33] P. J. Steinhardt, D. R. Nelson, and M. Ronchetti, Phys. Rev. B **28**, 784 (1983).
[34] Because a system of Lennard-Jones particles does not have a bcc or hcp phase, we instead prepared systems with the desired symmetry and then randomly displaced each particle by an amount $(2r-1)\delta$, where $\delta=0.12$ and r is a uniform random number between 0 and 1.
[35] L. Monette, W. Klein, and M. Zuckermann, J. Stat. Phys. **66**, 117 (1992).
[36] J. W. Cahn and J. E. Hilliard, J. Chem. Phys. **31**, 688 (1959).
[37] J. D. Gunton, P. Sahni, and M. S. san Miguel, in *Phase Transitions and Critical Phenomena*, edited by C. Domb and J. L. Lebowitz (Academic Press, New York, 1983), Vol. 8.
[38] K. Binder, Phys. Rev. A **29**, 341 (1984).
[39] D. W. Heermann, W. Klein, and D. Stauffer, Phys. Rev. Lett. **49**, 1262 (1982).
[40] N. Gulbahce, H. Gould, and W. Klein, Phys. Rev. E **69**, 036119 (2004).
[41] Some investigators (see, for example, Ref. [42]) refer to the value of the quench parameter at which the lifetime of the metastable state becomes less than some minimum value as the "spinodal." This limit of metastability is usually referred to as the Becker-Döring limit [37]. The more common definition of the spinodal refers to the value of the quench parameter at which the compressibility (susceptibility) diverges [37,38].
[42] A. C. Pan, T. J. Rappl, D. Chandler, and N. P. Balsara, J. Phys. Chem. B **110**, 3692 (2006). These workers observe nucleation in a three-dimensional Ising model with nearest-neighbor interactions and find that the size of the critical nucleus decreases monotonically as the quench depth is increased and is finite at the Becker-Döring limit. Because the interaction is short range, there are no spinodal effects in their system and we would not expect the compressibility and the critical droplet size to diverge.
[43] M. A. Novotny, W. Klein, and P. A. Rikvold, Phys. Rev. B **33**, 7729 (1986).
[44] N. Grewe and W. Klein, J. Math. Phys. **18**, 1735 (1977).
[45] W. Klein, H. Gould, N. Gulbahce, J. B. Rundle, and K. Tiampo, Phys. Rev. E **75**, 031114 (2007).
[46] C. Unger and W. Klein, Phys. Rev. B **29**, 2698 (1984).
[47] We can determine the temperature dependence of the mean number of particles in the nucleating droplet n_c near the spinodal from scaling arguments (see Ref. [45]). The density of the fundamental clusters near the spinodal is ϵ/G_s, where $\epsilon=(T-T_s)/T_s$, the Ginzburg parameter $G_s=R^d\epsilon^{3-d/2}$, and R is the effective range of the interaction. Because the nucleating droplet is formed by the coalescence of G_s fundamental clusters [45], n_c scales as $n_c \sim G_s(\epsilon/G_s)\xi^d=\epsilon R^d\epsilon^{-d/2}=R^d\epsilon^{1-d/2}$, where the correlation length ξ scales as $\xi\sim R\epsilon^{-1/2}$. We conclude that n_c diverges near the spinodal as $\epsilon^{-1/2}$ in three dimensions and remains constant (or diverges logarithmically) in two dimensions. The radius of gyration R_g scales as $R_g\sim\xi\sim R\epsilon^{-1/2}$ and diverges near the spinodal in all dimensions. Note that these scaling arguments do not predict how close the system has to be to the spinodal for the predicted behavior to be observed and assume that the nucleating droplet is spherical on average.